

Transmission in a Fano-Anderson chain with a topological defectRitu Nehra,^{1,2} Ajith Ramachandran,¹ Sebastian Wüster,¹ and Auditya Sharma¹¹*Department of Physics, Indian Institute of Science Education and Research, Bhopal, Madhya Pradesh 462066, India*²*Raman Research Institute, Bangalore, Karnataka 560080, India*

(Received 2 November 2020; revised 19 March 2021; accepted 22 March 2021; published 7 April 2021)

The Fano-Anderson chain consists of a linear lattice with a discrete side-unit, and it exhibits Fano-resonant scattering due to coupling between the discrete states of the side-unit and the tight-binding continuum. We study Fano-resonance-assisted transport for the case of a topologically nontrivial side unit. We find that the topology of the side-unit influences the transmission characteristics, which thus can be an effective detection tool of the topological phases of the side unit. Furthermore, we explore the role of dual links between the linear tight-binding chain and the side unit. The secondary connection between the main chain and the side-unit can modify the position or width of the Fano resonance dip in the transmission probability, and thus can yield additional control.

DOI: [10.1103/PhysRevB.103.155111](https://doi.org/10.1103/PhysRevB.103.155111)**I. INTRODUCTION**

Fano resonance [1,2] is a quantum phenomenon arising from the interaction between a continuum band of states and discrete states. It has been explored in a wide variety of settings, ranging from nuclear, atomic, molecular, and condensed-matter systems [3,4] to electronics [5,6] and optics [7–9]. Linear wave equations on Hamiltonian lattices can also give rise to Fano resonances if local defects are present [3,10]. The Fano-Anderson chain made up of a linear chain interacting with a single defect site is the simplest example for such a system [11]. The discrete state introduced by the defect allows additional propagation paths for scattering waves, which interfere constructively or destructively. This discrete-state-assisted interference may lead to perfect transmission or perfect reflection along with an asymmetric resonance profile.

Recent years have seen quickly growing interest in the exploration of Fano resonance associated with many different kinds of modified Fano-Anderson chains. Examples include systems with a single defect site [12,13], a linear chain [14], and a Fibonacci chain [15]. One common observation in all these structures is that the Fano resonance profile in the transmission probability shows a dip at the eigenenergies of the side unit interacting with the main chain. Since topological systems [16,17] are naturally endowed with isolated energy states, one expects interesting Fano scattering properties. Nonetheless, Fano resonances in such topological models have only very recently drawn attention [18], and it was shown that the Fano resonance profile could inherit topological protection against disorder. We study quite different aspects of such a setup, and we show that the topological features of the scattering side unit are reflected in the resonance profile, and this can in turn be utilized as a detection tool for topological systems.

Choosing the Su-Schrieffer-Heeger (SSH) chain, which is a prototype example of a topological model as the side unit, we demonstrate how the Fano transmission profile is affected

by the topological-to-trivial phase transition. The main motivation of our work is to explore the impact of edge states forming at the boundary between a trivial and a topological chain on the transport in the trivial chain. The SSH chain can be smoothly tuned across the trivial-to-topological phase with the aid of a control parameter in the Hamiltonian. In the trivial phase, we observe a perfect transmission at energies close to zero. As the SSH Hamiltonian is tuned to the topological phase, the isolated edge state emerging in the topological phase induces a Fano resonance and leads to a dip in the transmission profile at the energy of the edge state. One remarkable feature of the structure chosen is that the trivial-to-topological transition can be identified from the dip emerging in the transmission profile. This intriguing feature of the transmission profile may potentially lead to applications in switching devices [19,20].

Moreover, the fact that the boundary conditions of the topological systems modify the edge states naturally acts as an incentive to explore the effect of boundary conditions on transport. We observe that indeed the boundary conditions of the SSH chain alter the transmission profile in a striking manner. This concept can be further extended to two- or three-dimensional topological systems. We also explore the possibility of connecting the trivial and topological systems using two connections, and we observe that the second connection further produces characteristic changes in the transmission profile. Moreover, the second connection introduces additional possibilities of controlling the resonance width of the dips in the transmission profile. This feature may be potentially exploited in sensing devices [21].

In this article, we employ the transfer-matrix method (TMM) to study the transmission profile [11,22] of the Fano-Anderson chain, which allows for exact analytical expressions describing the transmission characteristics. The method has been used in the past to explore the Fano-Anderson chain with one connection to the side unit [3]. We focus on a linear chain with two connections to a topological side unit. We derive

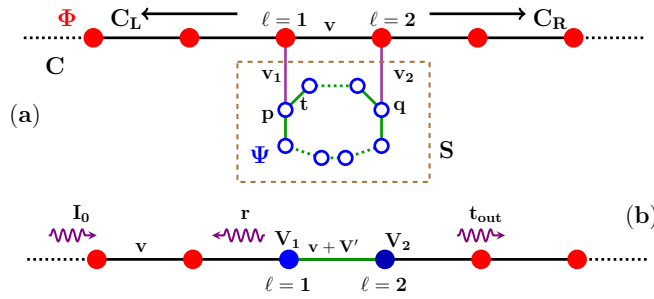


FIG. 1. (a) Schematic of the setup with two adjacent connections between the main chain (C) and the p th and q th sites of the side unit (S). These connections have hopping strengths v_1 and v_2 . The hopping amplitude in the main chain is set to v with on-site wave function Φ and hopping in the side unit t . We mark the left and right parts of the main chain as C_L and C_R and the side-unit as S for clarity. (b) Schematic representation of the Fano-Anderson chain with effective potentials V_1 and V_2 at sites $\ell = 1$ and 2 , respectively, which result after elimination of the side-unit. The effective hopping between these two sites becomes $v + V'$.

the exact expression for the transmission coefficient, and we obtain the conditions for perfect reflection. Our methods are general enough to be applicable to any kind of finite-sized side unit, which may be quasi-one-dimensional, two-dimensional, or even three-dimensional.

The manuscript is arranged as follows. In the next section, we describe the Fano-Anderson model, which is linked to a side unit with two adjacent connections. This section also describes how the transfer-matrix method can be used to obtain the conditions needed for Fano resonance. In Sec. III, we present the topological properties of the SSH model considering all possible structures. Further, in Sec. IV, we study Fano resonance in different cases of the SSH model taken as the side unit. Finally, we collect and summarize our findings in the Conclusion.

II. MODEL

We consider a linear tight-binding chain connected to a Fano defect chain with two connections between them as shown in Fig. 1. The Hamiltonian for this system is

$$H = H_c + H_s + H_{cs}, \quad (1)$$

where H_c is the Hamiltonian corresponding to the linear chain C ,

$$H_c = v \sum_{\ell} (\Phi_{\ell+1}^* \Phi_{\ell} + \Phi_{\ell}^* \Phi_{\ell+1}). \quad (2)$$

Here, Φ_{ℓ} is the complex wave amplitude at the site ℓ , and v is the coupling strength. H_s corresponds to the Hamiltonian for the side chain S with N sites, and it reads

$$H_s = \sum_{i,j=1}^N h_{i,j} \Psi_i^* \Psi_j, \quad (3)$$

where Ψ_i is the complex wave amplitude at the site i on the side chain, and h_{ij} is the coupling strength connecting the sites labeled i, j . The third term in the Hamiltonian H_{cs} corresponds

to the coupling between the main chain and the side chain, and it is given by

$$H_{cs} = v_1 \Phi_1^* \Psi_p + v_2 \Phi_2^* \Psi_q + \text{H.c.}, \quad (4)$$

with v_1 and v_2 being the coupling strengths between the main chain and the side chain. Sites p and q are arbitrary and can even be the same. In the absence of the side unit, Bloch's theorem can be applied to the translationally invariant linear chain C described by Eq. (2). For states $\phi_{\ell} = e^{i k \ell}$ one finds energies of propagating waves $E = 2v \cos k$, where k is the wave number. The side unit acts as a scatterer and introduces extra paths for an incoming wave. This resonant scattering due to the side unit controls the wave propagation in the main chain, and we employ the transfer-matrix method to obtain the transmission and reflection coefficients associated with the propagation in the main chain C in the presence of a side unit S .

The time (τ) dependence from the Schrödinger equation is eliminated using the ansatz

$$\Phi(\ell, \tau) = A_{\ell} e^{-i E \tau}, \quad (5)$$

$$\Psi(j, \tau) = B_j e^{-i E \tau}. \quad (6)$$

The time-independent Schrödinger equation corresponding to the Hamiltonian (H) can be written as

$$E A_{\ell} = v(A_{\ell+1} + A_{\ell-1}) + v_1 B_p \delta_{\ell,1} + v_2 B_q \delta_{\ell,2}, \quad (7)$$

$$E B_i = \sum_{j=1}^N h_{i,j} B_j + v_1 \delta_{i,p} A_1 + v_2 \delta_{i,q} A_2, \quad (8)$$

where Eqs. (7) and (8) correspond to sites in the main chain and the side unit, respectively. To obtain the transmission characteristics in the main chain, the two coupled equations must be solved simultaneously. The complex amplitudes B_i in the side unit can be written in terms of the amplitudes A_{ℓ} in the main chain as follows. Using Eq. (8), the relation between B_i and A_{ℓ} can be written as $\mathcal{H}_N \mathcal{B}_N = \mathcal{A}_N$, where $\mathcal{H}_N(E) = [EI - H_s]_{N \times N}$, $\mathcal{B}_N = [B_1, \dots, B_p, \dots, B_q, \dots, B_N]^T$, and $\mathcal{A}_N = [0, \dots, v_1 A_1, \dots, v_2 A_2, \dots, 0]^T$, with I the identity matrix and N the size of the side chain (S). Inverting the matrix \mathcal{H}_N [23], the expressions for $B_{p/q}$ now become

$$B_p = v_1 \alpha_{pp} A_1 + v_2 \alpha_{pq} A_2, \quad (9)$$

$$B_q = v_1 \alpha_{qp} A_1 + v_2 \alpha_{qq} A_2, \quad (10)$$

where $\alpha_{ij}(E) = [\mathcal{H}_N^{-1}(E)]_{ij}$. The Hermiticity of the Hamiltonian guarantees that $\alpha_{ij} = \alpha_{ji}^*$. These equations can be substituted back into Eq. (7) to obtain the wave propagation in the main chain in terms of the amplitudes A_{ℓ} as

$$E A_{\ell} = (\alpha_{pp} v_1^2 \delta_{\ell,1} + \alpha_{qq} v_2^2 \delta_{\ell,2}) A_{\ell} + (v + v_1 v_2 \alpha_{pq} \delta_{\ell,1}) A_{\ell+1} + (v + v_2 v_1 \alpha_{qp} \delta_{\ell,2}) A_{\ell-1}. \quad (11)$$

Equation (11) is the modified lattice equation for the main chain incorporating the effects of the scatterer in terms of effective energy-dependent potentials $V_1(E) = \alpha_{pp} v_1^2$, $V_2(E) = \alpha_{qq} v_2^2$, and $V'(E) = v_1 v_2 \alpha_{pq}$ as sketched in Fig. 1(b). The energy dependence of the effective potentials allows for resonant scattering and can cause complete transmission or complete reflection of the incoming wave as well as an asymmetric

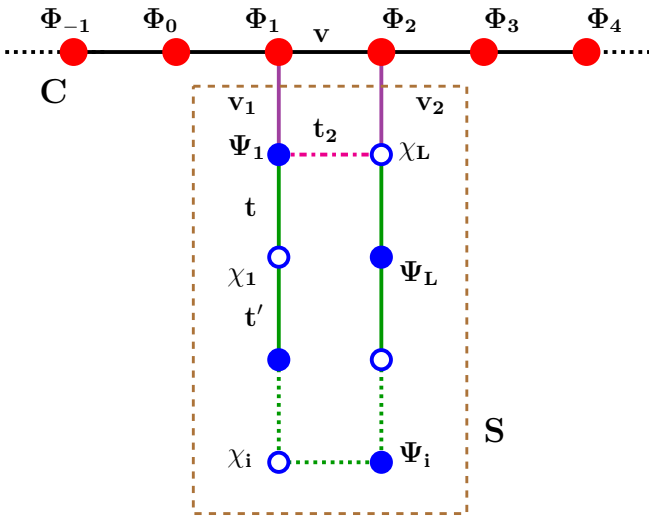


FIG. 2. Representation of the site amplitudes of wave functions, with the side unit described by a SSH model with intercell hopping t' and intracell hopping t . The main chain (C) hopping and the two connection hoppings are set to v , v_1 , and v_2 , respectively. The presence (absence) of the extra hopping $t_2 = t'$ with a dash-dotted magenta line turns the side unit into a closed (open) chain.

resonance profile. From Fig. 1(b), the condition for perfect reflection can be identified as $v = -V'(E)$ since the effective hopping between sites $\ell = 1$ and 2 would then vanish. In the limit $v_2 \rightarrow 0$, i.e., with just a single connection between the main chain and the side unit, $V_2(E)$ and $V'(E)$ vanish. Perfect transmission in this case occurs when $|\mathcal{H}_{N-1}| = 0$ or $V_1 = \alpha_{pp} = 0$, which results in a translationally invariant tight-binding chain with no effective scattering and therefore unit transmission. Perfect reflection is instead realized when $|\mathcal{H}_N| = 0$ or $V_1 = \alpha_{pp} = \infty$, i.e., an infinite on-site potential leads to full reflection or zero transmission [11].

Employing the transfer-matrix method (Appendix A) for Eq. (11), the transmission coefficient in terms of the energy of the incoming wave can be written as

$$T = \frac{v^2(4v^2 - E^2)|v + V'|^2}{[\beta v^2 + \gamma vE - E^2 M'_{11} M'_{22}]}, \quad (12)$$

where $\beta = (M'_{11} + M'_{22})^2 + (M'_{12} - M'_{21})^2$ and $\gamma = (M'_{11} - M'_{22})(M'_{12} - M'_{21})$ with $M'_{11} = [(E - V_1)(E - V_2) -$

$|v + V'|^2]$, $M'_{12} = -v(E - V_2)$, $M'_{21} = v(E - V_1)$, and $M'_{22} = -v^2$. When two side chain sites are simultaneously connected to the main chain, perfect reflection is possible if the energy is tuned in such a way that the condition

$$v + V' = 0 \quad (13)$$

holds, as can directly be seen in Eq. (12), besides the intuitive way of obtaining it from Fig. 1(b). The condition given in Eq. (13) is a consequence of destructive interference of the different paths available for the wave, which results in zero hopping amplitude for transmission across the scattering zone, leading to perfect reflection of the wave.

III. SSH CHAIN AND TOPOLOGY

In the discussion so far, details of the side unit did not enter. Now we choose the Su-Schieffer-Heeger (SSH) model as the side unit because of its interesting topological properties. The SSH model consists of a network of sites with alternating hopping amplitudes with the Hamiltonian given by

$$H_s^{\text{SSH}} = \sum_{i=1}^L (t\Psi_i^* \chi_i + t' \chi_i^* \Psi_{i+1}) + \text{H.c.}, \quad (14)$$

where Ψ_i, χ_i are the particle wave functions on two adjacent sites of the i th unit cell. For the case of our side unit, this is sketched in the dotted box of Fig. 2. The intracell coupling is labeled as t , whereas intercell coupling is t' .

The SSH model is known for its topological features. The winding number changes from 0 to 1 as the system is tuned from $t' < t$ to $t' > t$, indicating a phase transition from the topological phase to a trivial phase. The dispersion spectrum of the SSH model for a different total number of sites $N = 2L \pm 1$ or $2L$ is depicted in Fig. 3. A chain with an odd number of sites is incompatible with periodic boundary conditions. On the other hand, an open chain may have an odd or even number of sites and always gives rise to an edge state with energy $E \approx 0$ in the topological phase. The number of zero-energy edge states residing on the ends of the chain depends on the way the chain is terminated at the boundaries.

For an odd number of sites [Fig. 3(a)], there is always an edge state in the system. When $t' < t$ the edge state lies at the end with the hopping t' , whereas for $t' > t$ the edge state lies at the end with the hopping t of the SSH chain. The ratio

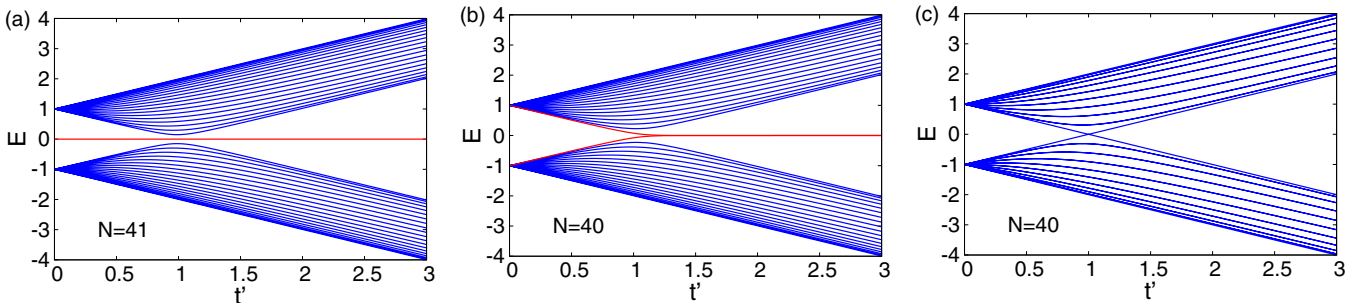


FIG. 3. The energy spectrum for the isolated SSH model with different intercell hopping t' and a constant intracell hopping $t = 1.0$ with red lines showing the energy of edge states. We show the spectrum for (a) $N = 2L \pm 1 = 41$ sites and (b) $N = 2L = 40$ sites with open boundary conditions and (c) $N = 2L = 40$ sites with periodic boundary conditions.

of the intracell to the intercell hopping ($\frac{t}{t'}$) of the SSH chain controls the position of this edge state. In contrast, for an even number of sites, edge states at both ends appear only when $t' > t$. The edge states present in the SSH model reside on the ends of the chain and decay in the bulk depending on the ratio of the intercell and intracell hopping ($\xi \propto \frac{t+t'}{t'-t}$). The system size should be greater than the decay length for the properties of the edge states to be observable.

IV. FANO RESONANCE: SSH CHAIN AS THE SIDE UNIT

After a review of the physics of the isolated SSH model, we now explore how coupling it to the main chain affects transport properties on that chain. Here, we take the side unit to be the SSH chain as shown in Fig. 2. The expression for $\Gamma_N = |\mathcal{H}_N(E)| = |E\mathcal{I} - H_s|$ is thus given by

$$\Gamma_N = |E\mathcal{I} - H_s| = \begin{vmatrix} E & -t & 0 & 0 & \cdots & -t_2 \\ -t & E & -t' & 0 & \cdots & 0 \\ 0 & -t' & E & -t & \cdots & \vdots \\ 0 & 0 & \ddots & \ddots & \ddots & -t_1 \\ -t_2 & 0 & 0 & \cdots & -t_1 & E \end{vmatrix}_{N \times N}, \quad (15)$$

where $N = 2L$ or $2L \pm 1$ is the number of sites in the SSH side unit (with L unit cells on the SSH chain), and t, t' are two alternate hoppings. Since t and t' alternate on the subdiagonal and superdiagonal of the tridiagonal matrix $[\mathcal{H}_N(E)]$, one has to write $t_1 = t$ or t' depending on the length N , while $t_2 = 0$ for an open chain and $t_2 = t'$ for a closed chain. While the length of the open chain may be odd or even, the closed chain is forced to have an even number of sites, because of geometrical constraints, as we will discuss later. We use $\Gamma_{N-j}^{\{\lambda_1, \lambda_2, \dots, \lambda_j\}}$ to represent the determinant of the square matrix with dimension $(N-j) \times (N-j)$ that is formed after the removal of the $\{\lambda_1, \lambda_2, \dots, \lambda_j\}$ th rows and columns from the matrix $[E\mathcal{I} - H_s]$ given in Eq. (15).

In the following subsections, we separately discuss how the system size of the side unit and whether the SSH chain is open or closed affects transport in the main chain. The properties of the open and closed SSH chains are quite different due to the presence and absence, respectively, of edge states. The focus of this study is on understanding how the transmission properties carry signatures of these edge states, which play a crucial role at energies close to zero ($E \sim 0$). Therefore, the first and last site (n th) of the SSH chain are connected to the main chain, as shown in Fig. 2.

A. Case 1: Open chain with odd N

We now discuss the transport properties of the system when the defect is the open SSH chain with an odd number of sites (Fig. 2). As discussed already, the open chain always possesses one edge state whose location depends on the relative hopping strengths t, t' as shown in Fig. 3(a). When $t' < t$, an edge state resides on the last site of the SSH chain and decays in the bulk, while in the other limit $t' > t$, the edge state resides on the first site. Besides varying the relative strength of t and t' , we have also considered two different cases for the second connection strength v_2 , i.e., $v_2 = 0$ and

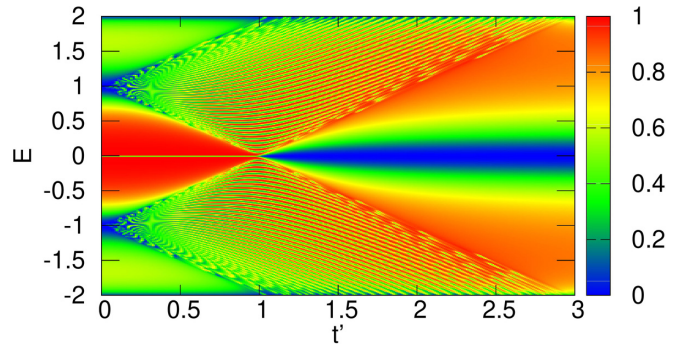


FIG. 4. The transmission coefficient T for the open SSH side chain with $N = 99$ for a single connection between chain and side unit. We show T as a function of intercell hopping t' and incoming wave energy E . The other parameters are kept constant: $v = 1, t = 1, v_1 = 1$, and $v_2 = 0$.

$v_2 \neq 0$. For all scenarios, we need to first evaluate the required coefficients of the inverse of the matrix \mathcal{H}_N . For the particular choice here, we have the relations $\alpha_{11} = \frac{\Gamma_{N-1}^{(1)}}{\Gamma_N}$, $\alpha_{nm} = \frac{\Gamma_{N-1}^{(n)}}{\Gamma_N}$, and $\alpha_{1n} = \alpha_{n1} = \frac{(tt')^{\frac{N-1}{2}}}{\Gamma_N}$.

First, we discuss the effect of a single link between the main chain and the side unit, i.e., $v_1 \neq 0; v_2 = 0$. For this scenario, perfect reflection ($T = 0$) results if $\Gamma_N = 0$ while perfect transmission ($T = 1$) is found for $\Gamma_{N-1}^{(1)} = 0$. Figure 4 features the transmission coefficient (T) as a function of the incoming energy of the wave function (E) and intercell hopping t' . It is observed that for $E = 0$, the system shows a clear perfect reflection for $t' > t$ with a broad blue region. However, for $t' < t$ a thin line is observed within the red region of full transmission as depicted in Fig. 4. The behavior of the transmission coefficient (T) in this case is consistent with the characteristics of the eigenstate of the full Hamiltonian at $E = 0$ as shown in Fig. 14 in Appendix B. In the limit $t' < t$, the eigenstate at $E = 0$ supports no probability amplitude in the main chain, and as a consequence a sharp dip indicating zero transmission is observed as shown in Fig. 4. In the limit $t' > t$, for the $E = 0$ state, the probability amplitude resides only on one-half of the main chain, and hence it leads to perfect reflection as indicated by the broad blue region in Fig. 4.

If the second coupling to the Fano defect side chain is added ($v_2 \neq 0$), the condition for perfect reflection is modified. It is now possible only for those energies that satisfy

$$v\Gamma_N + v_1 v_2 (tt')^{\frac{N-1}{2}} = 0, \quad (16)$$

where $\Gamma_N = \prod_{\theta_m} (E \pm \sqrt{t^2 + t'^2 + 2tt' \cos \theta_m})$ with $\theta_m = \frac{2\pi m}{N+1}; m = 1, 2, \dots, \frac{N-1}{2}$ [24]. The transmission coefficient as a function of the incoming wave energies and the intercell coupling t' is shown in Fig. 5. Full reflection is observed at $E = 0$ in both the regimes, $t' < t$ and $t' > t$. In both of the cases $t' > t$ as well as $t' < t$, the zero-energy wave propagates to the scattering region of the main chain and reflects back (verified from a study of the full system eigenstates shown in Fig. 15 in Appendix B). This finally results in minimum transmission through the system. Thus, the narrow line observed for $v_2 = 0$ with $t' < t$ in Fig. 4 is modified into a wider blue region when $v_2 \neq 0$, as shown in Fig. 5.

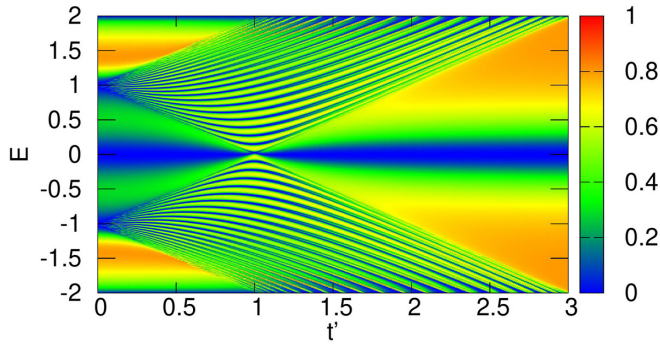


FIG. 5. Transmission as a function of the incoming wave energy E for the couplings between the main chain and the open SSH side chain with $N = 99$ for different intercell hoppings t' . The system parameters are set to $v_1 = 1$, $v_2 = 1$, $v = 1$, and $t = 1$.

We have seen that a connection v_2 to the side chain significantly modifies the transmission in the system. This motivates us to study how tuning the second coupling strength v_2 affects transmission for various interleg hopping strengths t' as shown in Fig. 6. We see that when $v_2 = 0$, for energy close to zero, the transmission is zero for any value of t' . However, for non-vanishing v_2 , the system shows transmission only in the limit $t' \rightarrow t$. As t' approaches t , the SSH chain starts to behave as a simple nearest-neighbor tight-binding chain, and for an odd system size it should show perfect reflection for energies $E \sim 0$. But due to the presence of the secondary connection, the energy corresponding to perfect reflection (shown in Fig. 18) is given by Eq. (16). Therefore, the system shows some transmission for energies close to zero, as shown in Fig. 6. In Appendix C, we discuss the role of the second connection, when the side unit is a simple tight-binding linear chain.

B. Case 2: Open chain with even N

Next we explore the SSH open chain with an even number of sites as the side chain. In this case, the isolated SSH model

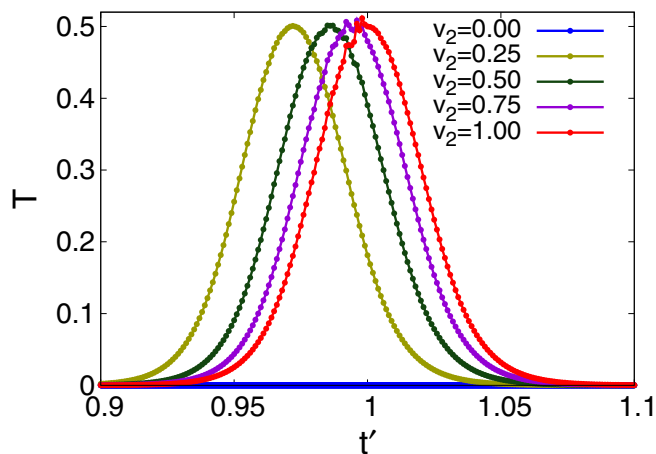


FIG. 6. The transmission coefficient as a function of different intercell hopping t' of the open SSH chain for different second connection strengths v_2 . The other system parameters are kept fixed: $N = 99$, $t = v = v_1 = 1$, and $E \sim 0$.

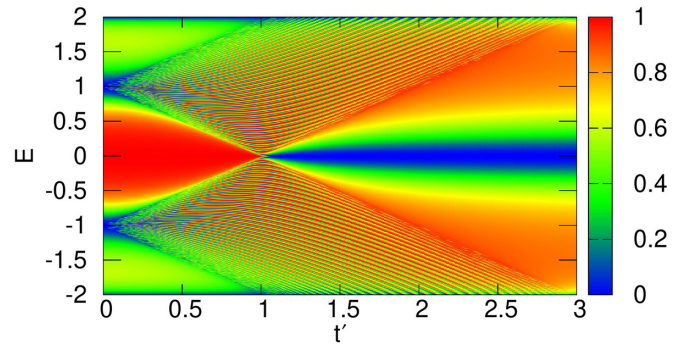


FIG. 7. The transmission coefficient (T) for a single coupling between the main chain and an open SSH side chain with $N = 100$ as a function of incoming wave energy E and intercell hoppings t' with other parameters set to $v = 1$, $t = 1$, $v_1 = 1$, and $v_2 = 0$.

possesses either no edge state (zero-energy state) for the case $t' < t$ or two edge states located at the two ends for the case $t' > t$ as shown in Fig. 3(b). To understand the transmission in this system, the required coefficients of the inverse matrix \mathcal{H}_N are calculated as $\alpha_{11} = \alpha_{nn} = \frac{\Gamma_{N-1}^{(1)}}{\Gamma_N}$, $\alpha_{1n} = \alpha_{n1} = \frac{(tt')^{\frac{N}{2}}}{t\Gamma_N}$. In the single coupling setup to the scattering center ($v_1 \neq 0$; $v_2 = 0$), the condition for perfect reflection ($T = 0$) is again given by $\Gamma_N = 0$ and the condition for perfect transmission is given by $\Gamma_{N-1}^{(1)} = 0$. The transmission spectrum as a function of incoming wave energy E and intercell hopping t' is shown in Fig. 7. At $E \sim 0$, the transmission coefficient undergoes a transition from 1 (red region) to 0 (blue region) on switching from the trivial (at $t' < t$) to the topological (at $t' > t$) phase of the SSH chain as shown in Fig. 7. The propagating wave reflects back from the scattering region in the main chain as depicted by the eigenstate of the full Hamiltonian in Fig. 16 (Appendix B).

The two links to the side chain modify the condition for perfect reflection, which now happens for energies satisfying the equation

$$vt'\Gamma_N + v_1v_2(tt')^{\frac{N}{2}} = 0, \quad (17)$$

where $\Gamma_N = \prod_{\theta_m} (E \pm \sqrt{t^2 + t'^2 + 2tt' \cos \theta_m})$. The variable θ_m is calculated numerically using the relation $t \Lambda(\theta_m, \frac{N}{2}) + t' \Lambda(\theta_m, \frac{N}{2} - 1) = 0$, where $\Lambda(\theta_m, l) = \frac{\sin[(l+1)\theta_m]}{\sin \theta_m}$ [24]. In the case $t' < t$, the wave propagates without disturbance in the main chain, which results in perfect transmission in the system. However, in the other limit $t' > t$, the main chain is connected to the two edge states of the SSH chain, and therefore, as shown in Fig. 8, minimum transmission is obtained due to the reflection of the incoming wave by these edge states (Fig. 17). Thus, the transmission coefficient T again features a transition from 1 to 0 for zero energy when the side chain undergoes a transition from the trivial to the topological phase, but the width of the perfect reflection area is increased in the presence of the secondary coupling v_2 . At $E = 0$, the transmission coefficient T is unaffected by the secondary connection to the side chain as shown in Fig. 8. This should be seen as a consequence of the robustness of the topologically protected edge states of the SSH chain.

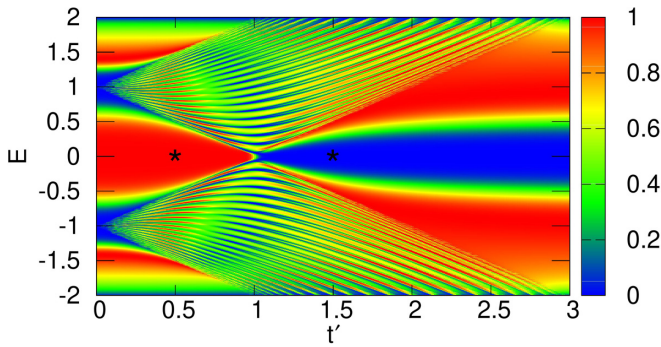


FIG. 8. The transmission coefficient T for the open SSH side chain with length $N = 100$ for two couplings (v_1, v_2) between the main chain and the side unit. We show T as a function of intercell hopping t' and incoming wave energy E . The other parameters are kept constant: $v = 1$, $t = 1$, $v_1 = 1$, and $v_2 = 1$. The wave amplitudes corresponding to the two (*) symbols are plotted in Fig. 9.

We verify the results by studying wave propagation using the time-dependent Schrödinger equation [25] in the system. The incoming wave is represented by an initial Gaussian wave packet (time $\tau = 0$) localized at a site l_0 (with $l_0 \ll l = 1$), which is far left of the scattering region. It can be written as

$$\psi(j) = e^{-ikj} e^{-\frac{1}{2}\left(\frac{j-l_0}{\sigma}\right)^2}, \quad (18)$$

where σ is the width and k is the momentum. The wave packet at a later time τ_0 can be obtained from the time-dependent Schrödinger's equation given by

$$\psi(j, \tau_0) = e^{-iH\tau_0} \psi(j, 0). \quad (19)$$

The initial wave packet evolves in time and moves toward the scattering region. The posts scattering features of the wave packet are governed by the Hamiltonian of the side unit. We focus on the wave amplitude in the system after the scattering when the energy of the incoming wave packet is $E = 0$ at two points indicated by star (*) symbols in Fig. 8. In Figs. 9(a) and 9(b) we show the square of the wave amplitude for $t' = 0.5$ and 1.5, respectively. In the trivial phase ($t' < t$), the entire wave packet is transmitted beyond the scattering region indicating complete transmission. In the topological phase $t' > t$, on the other hand, the wave packet is completely reflected from the scattering region. Thus, the dynamics reaffirms the results obtained from TMM, despite the finite energy width of the wave packet (18). This is enabled by the broad spectral width of the total reflection and total transmission features in Fig. 8 for $t' < t$ and $t' > t$, respectively.

Finally, we show the transmission coefficient as a function of t' for different values of v_2 in Fig. 10. The transmission coefficient shows a steplike drop from 1 to 0 as the system switches from the trivial to the topological phase at $t' = t$. Usually, this phase transition happens exactly at $t' = t$ only for large system sizes. However, Fig. 10 shows that the secondary connection facilitates this phase transition as the jump in T at $t' = t$ becomes sharp even for small system sizes. The combination of an energetically broad region of total reflection (for $t' < t$) and total transmission (for $t' > t$) evident in Fig. 8, with a fairly abrupt transmission between the two in terms of

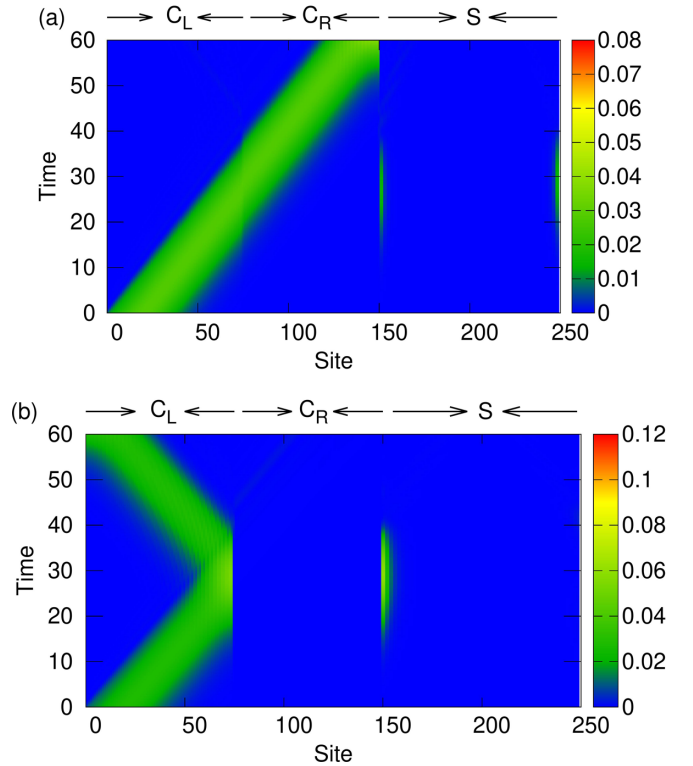


FIG. 9. The evolution of the square of the wave amplitude for an incoming wave packet with energy $E = 0$ in the system. The main chain (site = $1, 2, \dots, N_c$) with hopping $v = 1$ and length $N_c = 150$ is connected to an open SSH side chain (site = $N_c + 1, \dots, N_c + N$) of length $N = 100$ with couplings $v_1 = 1, v_2 = 1$. We mark the left and right parts of the main chain as C_L and C_R and the SSH side-unit as S for clarity. Here $t = 1$. (a) For $t' = 0.5$ we find perfect transmission and for (b) $t' = 1.5$ perfect reflection. The wave amplitudes correspond to the two (*) symbols shown in Fig. 8.

t' as seen in Fig. 10, might have useful switching applications for devices.

C. Case 3: Closed chain with even N

In this subsection, we look at the last case, namely the closed SSH chain with an even number of sites. In this

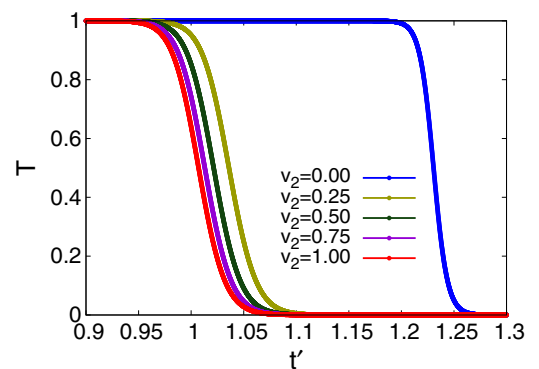


FIG. 10. The transmission coefficient as a function of different intercell hopping t' of the open SSH side chain for different second connection strengths v_2 with other system parameters fixed at $N = 100$, $t = v = v_1 = 1$, and $E \sim 0$.

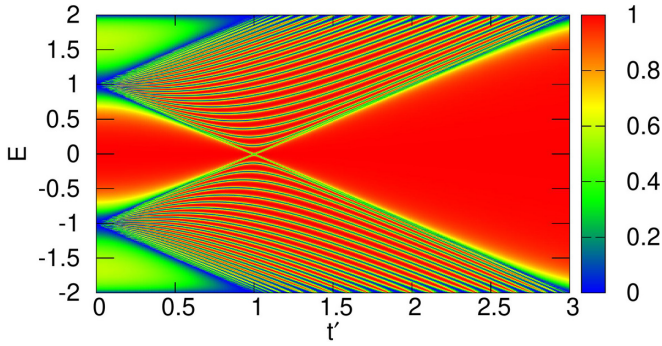


FIG. 11. The transmission (T) in the system for various incoming wave energies E and intercell couplings t' when a single connection exists between the main unit and a closed SSH side unit with length $N = 100$. The other parameters are kept constant: $v = 1$, $t = 1$, $v_1 = 1$, and $v_2 = 0$.

scenario, the ends of the side chain are connected to the main chain as well as to each other as shown in Fig. 2. The closed isolated SSH chain becomes gapless at $t' = t$ with the two energy bands touching at zero energy as depicted in Fig. 3(c). This results in non-zero-energy states in both regions $t' < t$ and $t' > t$. Here, the coefficients of the inverse of the matrix \mathcal{H}_N are given by $\alpha_{11} = \alpha_{nn} = \frac{\Gamma_{N-1}^{(1)}}{\Gamma_N}$, $\alpha_{1n} = \alpha_{n1} = \frac{(t')^{\frac{N}{2}} + t'^2 \Gamma_{N-2}^{(1,N)}}{t' \Gamma_N}$. The relation $\Gamma_N = \prod_{\theta_m} (E \pm \sqrt{t^2 + t'^2 + 2tt' \cos \theta_m})$ with $\theta_m = \frac{4m\pi}{N}$, $m = 1, 2, \dots, N/2$, yields Γ_N [24]. Figure 11 shows the behavior of the transmission coefficient T of the system in the presence of a single connection to the side chain in the two phases ($t' > t$ and $t' < t$) of the system. Again, perfect transmission is attained for the incoming energies satisfying $\Gamma_{N-1}^{(1)} = 0$, whereas perfect reflection is attained for energies consistent with $\Gamma_N = 0$ as shown in Fig. 11. The system shows full transmission for energies close to zero in both regions ($t' > t$ and $t' < t$) of the SSH chain due to the opening of the energy bands.

The addition of one more connection (v_2) further modifies the condition for perfect reflection, which now happens for energies consistent with

$$v\Gamma_N + v_1 v_2 t' \Gamma_{N-2}^{(1,N)} + v_1 v_2 (t')^{\frac{N}{2}} (t')^{\frac{N}{2}-1} = 0. \quad (20)$$

The behavior of the transmission coefficient in the presence of the two adjacent connections to the side chain is shown in Fig. 12. The transmission profile exhibits a change from perfect transmission to full reflection in the vicinity of the trivial-to-topological point as featured in Fig. 12. In the extreme case $t' \ll t$, the system shows full transmission, whereas in the other regime when $t' > t$, a suppression of transmission with increasing second coupling strength (v_2) is seen due to modified reflection conditions given by Eq. (20).

The behavior of the transmission for a range of secondary connection strengths for different interleg coupling t' is depicted in Fig. 13. In the absence of the second connection v_2 the transmission coefficient shows a sharp dip at the transition point $t' = t$. However, in the presence of the second connection v_2 the width of the dip at $t' = t$ is split into a dip and a peak in the vicinity of the transition point $t' = t$. This is due

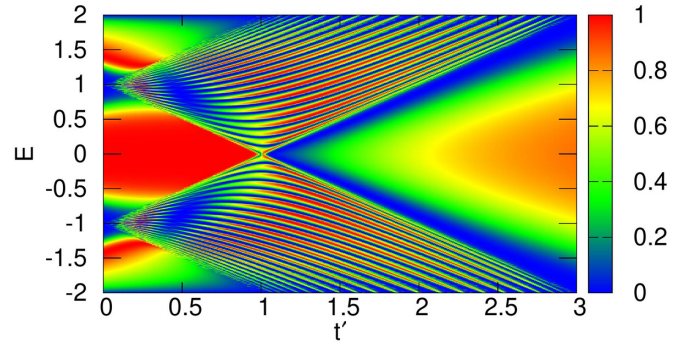


FIG. 12. The transmission coefficient T for the closed SSH side chain with $N = 100$ for double coupling between the main chain and the side unit. We show T as a function of intercell hopping t' and incoming wave energy E with other fixed system parameters as $v = 1$, $t = 1$, $v_1 = 1$, and $v_2 = 1$.

to the extra connection to the main chain, which modifies the transmission conditions in the system.

V. EXPERIMENTAL REALIZATION

In this section, we briefly discuss the possible experimental realization of our setup. One way to generate the Fano-Anderson chain structures discussed here is using optical lattices filled with ultracold atoms like rubidium (^{87}Rb) [26–28]. For strong lattices, these realize a tight-binding chain for the atoms, while when replacing direct tunneling with laser-assisted tunneling between some sites, alternating tunneling couplings as required here can be realized [29,30]. This technique can additionally be combined with employing superlattices [31]. The recent realization of interacting bosonic SSH chains using atomic trapping in optical tweezers along with excitation to Rydberg states is an important development in the field [32,33].

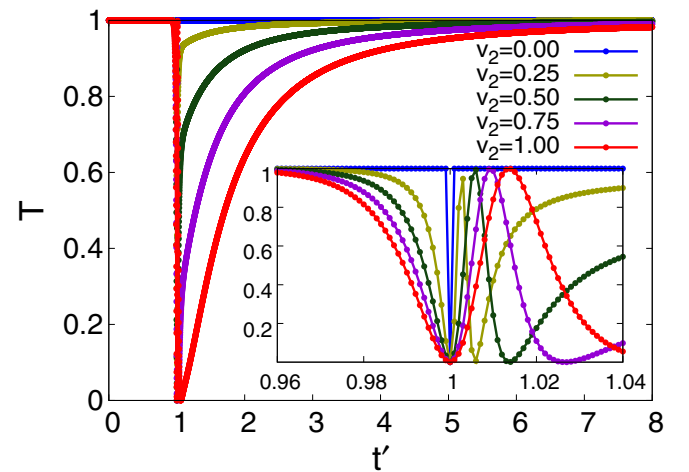


FIG. 13. The transmission coefficient as a function of different intercell hopping t' of the closed SSH side chain for different second connection strengths v_2 . The other system parameters are kept fixed at $N = 100$, $t = v = v_1 = 1$, and $E \sim 0$. The inset is a zoomed version that highlights the intricate structure in the vicinity of the phase-transition point.

A second platform where our results are directly applicable is photonic crystals [34,35]. Photonic crystal technology is based on the creation of nanocavities with a photonic band gap [36–38], which are introduced into a photonic crystal waveguide. These exclusion zones can then practically mimic a tight-binding chain for photons, where control over the coupling strengths can be exerted by adjusting the spacing between the sites. Recently, an SSH model with a combination of rigid and elastic materials, which could continuously be tuned across its topological phase transition by stretching [19], was proposed. By immersing the photonic crystal into a nematic liquid crystal background, dynamical tunability with the help of an external electric field could also be achieved [39].

VI. CONCLUSION

In this work, we analyze the interplay of Fano resonances, topology, and edge states in a Fano-Anderson chain possessing a topological side unit. We take the SSH chain, which possesses topological characteristics as a prototype side unit, and we show that the topology of the side unit modifies the Fano resonance profile and thus the transport probability past the topological unit. We observe that the transmission profile is modified when the system is tuned from the trivial to the topological phase. With a single connection between the main chain and the side unit, the topological to trivial transition cannot be efficiently detected. However, if two connections are present, a clear signal of the transition is obtained directly from the transmission profile. We provide a detailed study of how the transmission profile depends on the boundary conditions and the topological properties of the SSH chain. The detection of topological characteristics from Fano resonances in quantum transport could allow a new experimental handle on topological states.

We explicitly derive an exact expression for the transmission coefficient using the transfer matrix method, and we obtain conditions for Fano resonance as well as perfect reflection. The expression obtained can be generalized to an arbitrary side unit and hence may find application in other studies of Fano resonance assisted transport. This enables us to show that an open topological chain with an even number of sites exhibits a sharp transition between complete reflection or complete transmission of all waves with energy near zero, depending on the parameters of the topological scatterer. The sharpness of this transition paired with its wide bandwidth should make this a useful feature for switching in device applications involving photonic crystals or nanomaterials with topological elements.

Losses are inevitable in any physical system. Our preliminary check on weak losses incorporated in this system shows no significant changes in the transmission characteristics. The Fano resonance condition being the central pillar for determining the transmission characteristics, any sorts of losses that can preserve the resonance condition are admissible. Moreover, losses can be brought under control if they are weak enough, as reported in many experimental studies [40–42].

One of the intriguing features of the Fano assisted transmission profile is the narrow linewidth of the resonance,

which could provide high sensitivity in sensing systems. In the proposed Fano-Anderson chain, the two connections between the main chain and the side unit yield multiple choices for the tunability of the resonance width. The trivial to topological transition could be utilized for switching purposes since the sharp change in the transmission amplitudes at the resonant peak and dip is vital for such applications. Further, Fano resonance based photonic devices could potentially be employed for a variety of filters and interferometer devices, paving the way for further development of all-optical transistors, switches, and logical gates [3,20,21,43,44].

ACKNOWLEDGMENTS

A.S. acknowledges financial support from SERB via a grant (File No. CRG/2019/003447), and from DST via the DST-INSPIRE Faculty Award (DST/INSPIRE/04/2014/002461).

APPENDIX A: TRANSMISSION COEFFICIENT

We assume that an incoming wave from the far left approaches the scattering region in the main chain, and that after the scattering time period, the wave has been split into two parts in the main chain: a reflected part moving toward the left and a transmitted part moving toward the right, as shown in Fig. 1(b). The boundary conditions for the stationary scattering states in the time-independent scattering problem can be written as

$$A_\ell = I_0 e^{ik\ell} + r e^{-ik\ell} \quad (\text{A1})$$

for $\ell < 1$ and

$$A_\ell = t_{\text{out}} e^{ik\ell} \quad (\text{A2})$$

for $\ell > 2$. The coefficients corresponding to the incoming, reflected, and transmitted waves are denoted, respectively, as I_0 , r , and t_{out} . We can now formulate a transfer matrix that connects the wave function on nearby sites of the main chain represented by the lattice Eq. (11) as

$$\begin{bmatrix} A_{\ell+1} \\ A_\ell \end{bmatrix} = M_T \begin{bmatrix} A_\ell \\ A_{\ell-1} \end{bmatrix}, \quad (\text{A3})$$

where M_T is the transfer matrix given by

$$M_T = \begin{bmatrix} \frac{E - \alpha_{pp} v_1^2 \delta_{\ell,1} - \alpha_{qq} v_2^2 \delta_{\ell,2}}{v + v_1 v_2 \alpha_{pq} \delta_{\ell,1}} & -\frac{v + v_2 v_1 \alpha_{qp} \delta_{\ell,2}}{v + v_1 v_2 \alpha_{pq} \delta_{\ell,1}} \\ 1 & 0 \end{bmatrix}. \quad (\text{A4})$$

As depicted in Fig. 1, the side unit and main chain are linked by two connections with different hopping v_1 and v_2 . Hence, we can represent the final transfer matrix of the system as a product of two transfer matrices at the two connecting sites. The first transfer matrix for the connection at the first site $\ell = 1$ is given by $M_1 = (M_T)_{\ell=1}$ and the second transfer matrix for the connection at the next site $\ell = 2$ is given by $M_2 = (M_T)_{\ell=2}$. Thus, the final transfer matrix is given by $M = M_2 M_1$, which connects wave functions of the parts that lie to the left and right of the scattering regions as

$$\begin{bmatrix} A_3 \\ A_2 \end{bmatrix} = M \begin{bmatrix} A_1 \\ A_0 \end{bmatrix} = M_2 M_1 \begin{bmatrix} A_1 \\ A_0 \end{bmatrix} \quad (\text{A5})$$

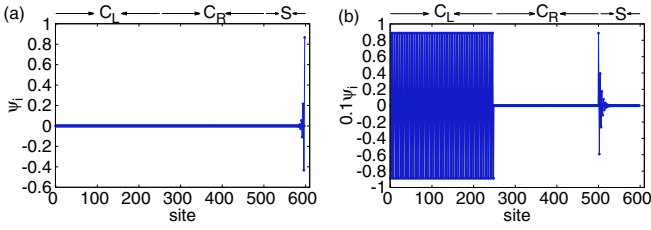


FIG. 14. The zero-energy wave function of the system when the main chain is the simple tight-binding chain with length $N_c = 500$ (corresponding to site indices running from 1 to 500) to which an open SSH side chain of length $N = 99$ (whose site indices run from 501 to 599) is connected to one of the two middle sites. We mark the left and right parts of the main chain as C_L and C_R and the SSH side-unit as S for clarity. The connecting hopping strengths are $v_1 = 1.0$, $v_2 = 0$ and the other parameters are $v = 1.0$, $t = 1.0$ with (a) $t' = 0.5$ and (b) $t' = 1.5$.

with

$$M = \begin{bmatrix} M_{11} & M_{12} \\ M_{21} & M_{22} \end{bmatrix}, \quad (\text{A6})$$

where $M_{ij} = \frac{M'_{ij}}{v(v+V')}$ with $M'_{11} = [(E - V_1)(E - V_2) - |v + V'|^2]$, $M'_{12} = -v(E - V_2)$, $M'_{21} = v(E - V_1)$, and $M'_{22} = -v^2$. Thus, the final transfer matrix for the setup is given by M .

The transmission coefficient $T = |t_{\text{out}}^2/I_0^2|$ is calculated from the transfer matrix using the boundary conditions [Eqs. (A1) and (A2)] as

$$T = \frac{4 \sin^2 k}{|M_{11}e^{-ik} + M_{12} - M_{21} - M_{22}e^{ik}|^2}. \quad (\text{A7})$$

Also, the transmission coefficient in terms of the energy of the incoming wave can be written as

$$T = \frac{v^2(4v^2 - E^2)|v + V'|^2}{[\beta v^2 + \gamma vE - E^2 M'_{11} M'_{22}]}, \quad (\text{A8})$$

where $\beta = (M'_{11} + M'_{22})^2 + (M'_{12} - M'_{21})^2$ and $\gamma = (M'_{11} - M'_{22})(M'_{12} - M'_{21})$.

APPENDIX B: WAVE FUNCTIONS FOR THE EDGE STATES

Here, we discuss the eigenstates of the complete Hamiltonian, which incorporates the main chain as well as the side SSH chain. The properties of a wave traveling in the main chain with a particular energy are intimately connected to these eigenstates of the complete Hamiltonian. We focus on the eigenstates corresponding to the energies at which a Fano resonance dip is observed in the transmission profile.

Figure 14 features the edge states of the system with a single connection ($v_1 \neq 0$ and $v_2 = 0$) between the main chain and the SSH chain possessing an odd number of sites. In the region $t' < t$, the edge state of the isolated SSH chain lies predominantly on the edge site of the chain, and the probability amplitude decays toward the bulk. The state at zero energy of the full system also shows the same behavior as depicted in Fig. 14(a). The eigenstate covers only a few sites close to the free end of the SSH chain, and no probability amplitude

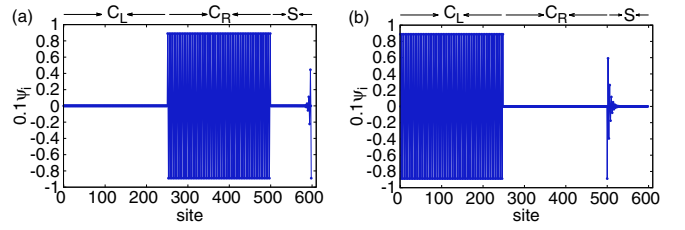


FIG. 15. The zero-energy wave function of the system when the main chain is the simple tight-binding chain with $N_c = 500$ (site indices running from 1 to 500) to which an open SSH chain of length $N = 99$ (whose site indices run from 501 to 599) is connected to one of the middle sites and an adjacent site. The connecting hopping strengths are $v_1 = 1.0$, $v_2 = 1.0$ and the other parameters are $v = 1.0$, $t = 1.0$, and (a) $t' = 0.5$ and (b) $t' = 1.5$.

is seen in the main chain. We would therefore expect no contribution to transport from this eigenstate, and thus a very sharp dip is observed in the transmission profile at $E = 0$. The eigenstates close to $E = 0$ are completely different as they possess probability amplitudes on the main chain (both toward the left and right of the defect) and allow a finite amount of transmission (Fig. 4).

In the region $t' > t$, the edge state mainly lies on the connected end of the SSH chain and decays in the bulk of the SSH chain. The connected end shows edge-state character here, despite its connection to the main chain. However, the amplitude at this end of the SSH chain is much smaller than in the other case in Fig. 14(a), which is similar to the edge state of the isolated SSH chain. Furthermore, as shown in Fig. 14(b), the eigenstate for the full system also shows a finite probability amplitude in the main chain that is to the left of the defect. We take an even total number of sites in the main chain so that the number of sites to the left of the defect is different from the number of sites to the right of the defect, thus breaking the left-right symmetry. As the eigenstate lies merely on one side of the main chain, zero transmission at this energy is observed as depicted in Fig. 4.

Next, we explore the eigenstate of the full system with two connections ($v_1 \neq 0$, $v_2 \neq 0$) between the side chain and the main chain (Fig. 15). In Fig. 15 we show the eigenstate corresponding to $E = 0$ for both cases $t' > t$ and $t' < t$. In both cases, the eigenstate of the full system vanishes in one-half of the main chain. As a consequence of this, again the transmission in the system is fully suppressed as shown in Fig. 5. With the double coupling, both ends of the SSH chain are connected to the main chain. We observe that a finite probability amplitude is seen at (a different) one of the edges in the two phases.

The isolated SSH open chain with an even number of sites shows zero modes only when $t' > t$, and so we look at the case $t = 1.0$, $t' = 1.5$. The system now possesses two zero-energy states (which are primarily represented at the two edges). Figure 16 shows the site coefficients of the two zero-energy eigenstates for the full Hamiltonian containing the main chain and the side chain, with a single connection v_1 between them. We observe that both of these states possess a finite probability amplitude in one part of the main chain and also at the free end of the SSH chain, as shown in Fig. 16. The zero amplitude

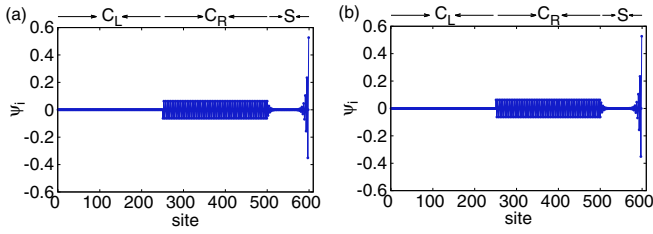


FIG. 16. The wave function for the two zero-energy states with a simple tight-binding chain with $N_c = 500$ (site indices running from 1 to 500) as a main chain and an open SSH chain with $N = 100$ (site indices running from 501 to 600) as a side chain, which is connected to one of the middle sites. The connecting hopping strengths are $v_1 = 1.0$, $v_2 = 0$ and other parameters are $v = 1.0$, $t = 1.0$, and $t' = 1.5$.

of the eigenstate in one-half of the main chain confirms the full reflection in the system corresponding to this energy, as depicted in Fig. 7.

The presence of the second connection v_2 leaves no free end for the SSH chain. Thus, the eigenstate for the full system is modified as shown in Fig. 17. The majority of the probability amplitude lies on one-half of the main chain, which results in zero transport in the system, as depicted in Fig. 8.

APPENDIX C: NEAREST-NEIGHBOR TIGHT-BINDING OPEN CHAIN AS A SIDE UNIT

We consider a nearest-neighbor tight-binding chain with hopping t (i.e., $t = t'$) coupled to the main chain with two connections v_1 and v_2 . The transmission coefficient (T) as a function of incoming wave energies (E) is shown in Figs. 18 and 19 for different secondary connection strength v_2 when the side unit possesses one ($N = 1$) and two ($N = 2$) sites, respectively.

In the absence of v_2 , the system shows a minimum transmission ($T = 0$) at $E = 0$ when the side unit contains an odd number of sites as the condition $\Gamma_N = 0$ is satisfied. For an even number of sites in the side chain, the system shows a maximum transmission ($T = 1$) at $E = 0$ as the condition $\Gamma_{N-1}^{(1)} = 0$ is satisfied.

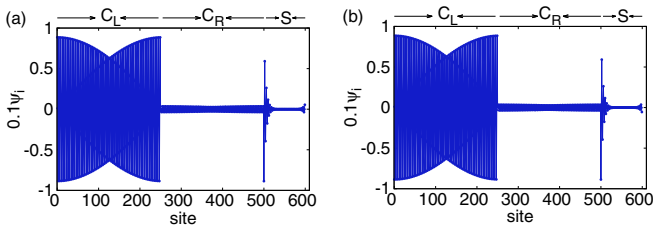


FIG. 17. The wave function for the two zero-energy states for a system consisting of a simple tight-binding chain with $N_c = 500$ (site indices running from 1 to 500) as a main chain and an open SSH chain with $N = 100$ (site indices running from 501 to 600) as a side chain, which is connected to one of the middle sites and an adjacent site. The connecting hopping strengths are $v_1 = 1.0$, $v_2 = 1.0$ and the other parameters are $v = 1.0$, $t = 1.0$, and $t' = 1.5$.

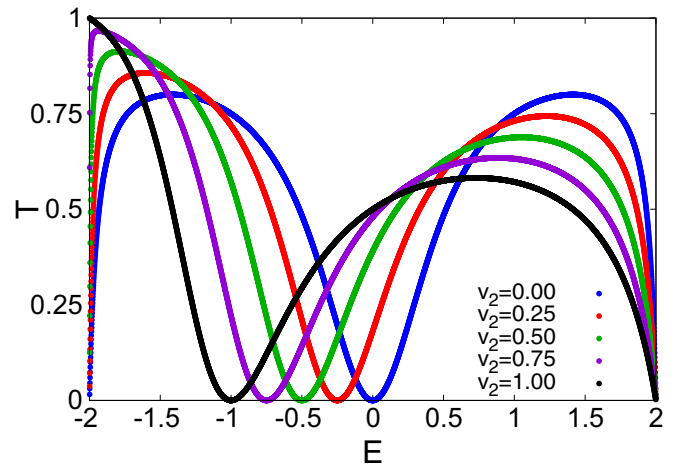


FIG. 18. Transmission coefficient as a function of the incoming wave energy with various second connection strengths v_2 when the main chain is the simple tight-binding chain and the side unit is a single site. The parameters are $v = 1.0$, $v_1 = 1.0$, and $t = 1.0$.

In the presence of the second connection v_2 , the perfect reflection condition is given by

$$v\Gamma_N + v_1v_2t^{N-1} = 0, \quad (\text{C1})$$

where $\Gamma_N = \prod_k [E - 2t \cos(k)]$ with $k = \frac{j\pi}{N+1}$; $j = 1, \dots, N$ with N being the side chain length.

If a single defect site is connected to the main chain through two connections v_1 and v_2 , then the position of the minimum of transmission is shifted by $-v_2$ (Fig. 18) according to Eq. (C1). Again invoking (C1) for $N = 2$, as v_2 is increased, the minima at $E = \pm 1$ move toward each other as shown in Fig. 19. Thus, the maximum at $E = 0$ for $v_2 = 0$ turns into a minimum for $v_2 = 1$.

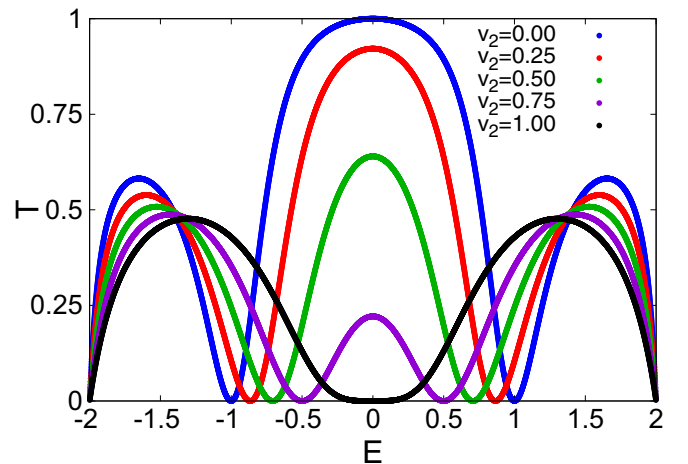


FIG. 19. Transmission coefficient as a function of incoming wave energy with various second connection strengths v_2 when the main chain is the simple tight-binding chain and the side unit is a two-site chain. The other parameters are $v = 1.0$, $v_1 = 1.0$, and $t = 1.0$.

- [1] U. Fano, Sullo spettro di assorbimento dei gas nobili presso il limite dello spettro d'arco, *Il Nuovo Cimento* **12**, 154 (1935).
- [2] U. Fano, Effects of configuration interaction on intensities and phase shifts, *Phys. Rev.* **124**, 1866 (1961).
- [3] A. E. Miroshnichenko, S. Flach, and Y. S. Kivshar, Fano resonances in nanoscale structures, *Rev. Mod. Phys.* **82**, 2257 (2010).
- [4] O. Újsághy, J. Kroha, L. Szunyogh, and A. Zawadowski, Theory of the Fano Resonance in the STM Tunneling Density of States Due to a Single Kondo Impurity, *Phys. Rev. Lett.* **85**, 2557 (2000).
- [5] S. Rotter, F. Libisch, J. Burgdörfer, U. Kuhl, and H.-J. Stöckmann, Tunable Fano resonances in transport through microwave billiards, *Phys. Rev. E* **69**, 046208 (2004).
- [6] A. Attaran, S. D. Emami, M. R. K. Soltanian, R. Penny, S. W. Harun, H. Ahmad, H. A. Abdul-Rashid, M. Moghavvemi *et al.*, Circuit model of fano resonance on tetramers, pentamers, and broken symmetry pentamers, *Plasmonics* **9**, 1303 (2014).
- [7] P. Fan, Z. Yu, S. Fan, and M. L. Brongersma, Optical fano resonance of an individual semiconductor nanostructure, *Nat. Mater.* **13**, 471 (2014).
- [8] C. Argyropoulos, F. Monticone, G. D'Aguzzo, and A. Alù, Plasmonic nanoparticles and metasurfaces to realize fano spectra at ultraviolet wavelengths, *Appl. Phys. Lett.* **103**, 143113 (2013).
- [9] F. Shafiei, F. Monticone, K. Q. Le, X.-X. Liu, T. Hartsfield, A. Alù, and X. Li, A subwavelength plasmonic metamolecule exhibiting magnetic-based optical fano resonance, *Nat. Nanotechnol.* **8**, 95 (2013).
- [10] A. Ramachandran, C. Danieli, and S. Flach, Fano resonances in flat band networks, *Fano Resonances in Optics and Microwaves* (Springer, Cham, 2018), pp. 311–329.
- [11] A. E. Miroshnichenko and Y. S. Kivshar, Engineering Fano resonances in discrete arrays, *Phys. Rev. E* **72**, 056611 (2005).
- [12] S. Longhi, Bound states in the continuum in a single-level fano-anderson model, *Eur. Phys. J. B* **57**, 45 (2007).
- [13] E. N. Bulgakov and A. F. Sadreev, Resonance induced by a bound state in the continuum in a two-level nonlinear Fano-Anderson model, *Phys. Rev. B* **80**, 115308 (2009).
- [14] A. Chakrabarti, Fano resonance in discrete lattice models: Controlling lineshapes with impurities, *Phys. Lett. A* **366**, 507 (2007).
- [15] A. Chakrabarti, Electronic transmission in a model quantum wire with side-coupled quasiperiodic chains: Fano resonance and related issues, *Phys. Rev. B* **74**, 205315 (2006).
- [16] L. Lu, J. D. Joannopoulos, and M. Soljačić, Topological photonics, *Nat. Photon.* **8**, 821 (2014).
- [17] P. St-Jean, V. Goblot, E. Galopin, A. Lemaître, T. Ozawa, L. Le Gratiet, I. Sagnes, J. Bloch, and A. Amo, Lasing in topological edge states of a one-dimensional lattice, *Nat. Photon.* **11**, 651 (2017).
- [18] F. Zangeneh-Nejad and R. Fleury, Topological Fano Resonances, *Phys. Rev. Lett.* **122**, 014301 (2019).
- [19] E. S. G. Naz, I. C. Fulga, L. Ma, O. G. Schmidt, and J. van den Brink, Topological phase transition in a stretchable photonic crystal, *Phys. Rev. A* **98**, 033830 (2018).
- [20] M. F. Limonov, M. V. Rybin, A. N. Poddubny, and Y. S. Kivshar, Fano resonances in photonics, *Nat. Photon.* **11**, 543 (2017).
- [21] H. Lu, X. Liu, D. Mao, and G. Wang, Plasmonic nanosensor based on fano resonance in waveguide-coupled resonators, *Opt. Lett.* **37**, 3780 (2012).
- [22] P. Tong, B. Li, and B. Hu, Wave transmission, phonon localization, and heat conduction of a one-dimensional Frenkel-Kontorova chain, *Phys. Rev. B* **59**, 8639 (1999).
- [23] J. R. Westlake, *A Handbook of Numerical Matrix Inversion and Solution of Linear Equations* (Wiley, New York, 1968), Vol. 767.
- [24] J. Sirker, M. Maiti, N. P. Konstantinidis, and N. Sedlmayr, Boundary fidelity and entanglement in the symmetry protected topological phase of the ssh model, *J. Stat. Mech.: Theor. Exp.* (2014) P10032.
- [25] J. J. Sakurai, *Modern Quantum Mechanics* (Addison-Wesley, New York, 1985).
- [26] M. Theis, Ph.D. thesis, Universit at Innsbruck, Austria, 2005.
- [27] S. Krinner, T. Esslinger, and J.-P. Brantut, Two-terminal transport measurements with cold atoms, *J. Phys.: Condens. Matter* **29**, 343003 (2017).
- [28] C. Gross and I. Bloch, Quantum simulations with ultracold atoms in optical lattices, *Science* **357**, 995 (2017).
- [29] H. Miyake, G. A. Siviloglou, C. J. Kennedy, W. C. Burton, and W. Ketterle, Realizing the Harper Hamiltonian with Laser-Assisted Tunneling in Optical Lattices, *Phys. Rev. Lett.* **111**, 185302 (2013).
- [30] M. Aidelsburger, M. Atala, M. Lohse, J. T. Barreiro, B. Paredes, and I. Bloch, Realization of the Hofstadter Hamiltonian with Ultracold Atoms in Optical Lattices, *Phys. Rev. Lett.* **111**, 185301 (2013).
- [31] F. Gerbier and J. Dalibard, Gauge fields for ultracold atoms in optical superlattices, *New J. Phys.* **12**, 033007 (2010).
- [32] S. de Léséleuc, V. Lienhard, P. Scholl, D. Barredo, S. Weber, N. Lang, H. P. Büchler, T. Lahaye, and A. Browaeys, Observation of a symmetry-protected topological phase of interacting bosons with rydberg atoms, *Science* **365**, 775 (2019).
- [33] V. Lienhard, S. de Léséleuc, P. Scholl, D. Barredo, T. Lahaye, and A. Browaeys, Experimental realization of a bosonic version of the su-schrieffer-heeger (ssh) model with rydberg atoms, in *Quantum Information and Measurement (QIM) V: Quantum Technologies* (Optical Society of America, Rome, 2019), p. F4B.2.
- [34] K. Inoue and K. Ohtaka, *Photonic Crystals: Physics, Fabrication and Applications* (Springer Science & Business Media, New York, 2004), Vol. 94.
- [35] Su-P. Yu, J. A. Muniz, C.-L. Hung, and H. J. Kimble, Two-dimensional photonic crystals for engineering atom-light interactions, *Proc. Natl. Acad. Sci. (USA)* **116**, 12743 (2019).
- [36] E. Kuramochi, Manipulating and trapping light with photonic crystals from fundamental studies to practical applications, *J. Mater. Chem. C* **4**, 11032 (2016).
- [37] K. Busch, S. F. Mingaleev, A. Garcia-Martin, M. Schillinger, and D. Hermann, The wannier function approach to photonic crystal circuits, *J. Phys.: Condens. Matter* **15**, R1233 (2003).
- [38] A. H. Safavi-Naeini and O. Painter, Design of optomechanical cavities and waveguides on a simultaneous bandgap phononic-photonic crystal slab, *Opt. Express* **18**, 14926 (2010).
- [39] M. I. Shalaev, S. Desnani, W. Walasik, and N. M. Litchinitser, Reconfigurable topological photonic crystal, *New J. Phys.* **20**, 023040 (2018).

- [40] D. Barredo, H. Labuhn, S. Ravets, T. Lahaye, A. Browaeys, and C. S. Adams, Coherent Excitation Transfer in a Spin Chain of Three Rydberg Atoms, *Phys. Rev. Lett.* **114**, 113002 (2015).
- [41] H. Labuhn, D. Barredo, S. Ravets, S. De Léséleuc, T. Macrì, T. Lahaye, and A. Browaeys, Tunable two-dimensional arrays of single rydberg atoms for realizing quantum ising models, *Nature (London)* **534**, 667 (2016).
- [42] M. Ludwig and F. Marquardt, Quantum Many-Body Dynamics in Optomechanical Arrays, *Phys. Rev. Lett.* **111**, 073603 (2013).
- [43] A. C. Johnson, C. M. Marcus, M. P. Hanson, and A. C. Gossard, Coulomb-Modified Fano Resonance in a One-Lead Quantum Dot, *Phys. Rev. Lett.* **93**, 106803 (2004).
- [44] M. E. Torio, K. Hallberg, S. Flach, A. E. Miroshnichenko, and M. Titov, Spin filters with fano dots, *Eur. Phys. J. B* **37**, 399 (2004).